SOI-Based 2-D MEMS L-Switching Matrix for Optical Networking

Tze Wei Yeow, *Member, IEEE*, K. L. Eddie Law, *Member, IEEE*, and Andrew A. Goldenberg, *Fellow, IEEE*

***Abstract*—Two-dimensional microelectromechanical system (2-D MEMS) optical switches have been widely demonstrated in research laboratories and in the industry. The limitations of 2-D MEMS switches are well known. The non-uniformity in losses due to differences in free space path lengths between the most and least distance paths among ports restrict(s) 2-D MEMS switches to a practical maximum port-count of 32 × 32. This problem has never been addressed. A novel switching architecture, L-switching matrix, that decreases the most distance free space path length and the difference between the most and least distance paths while maintaining same nonblocking port switching capacity has been proposed and demonstrated. Collimators with optimized beam waist are selected such that the insertion loss of the average beam path is the lowest. Larger beam waists are used to accommodate for the diffraction effects of the Guassian beam of the most distance path. However, larger beam waists require larger mirror areas to avoid beam-clipping and losses due to angular misalignment are more acute. Therefore, having shorter absolute and relative path lengths will avoid the beam-clipping effects and increase the port-to-port loss uniformity of the optical switch. The unique architecture of L-switching matrix which utilizes double-sided mirror can theoretically increase the maximum port-count to 64 × 64 or decrease the current insertion loss of a 32 × 32 MEMS switch by 50%. Moreover, L-switching matrix requires 25% less mirrors and electrodes than conventional cross bar architecture. A fabrication process involving silicon-on-insulator SOI wafers has been defined to fabricate the double-sided mirrors used in L-switching matrix.**

***Index Terms*—Innerconnect architecture, microelectromechanical system (MEMS), micromachined, optical crossconnect, optical switches.**

I. INTRODUCTION

THERE are currently two popular switching architectures in microelectromechanical system (MEMS) optical switching: 1) two-dimensional (2-D) MEMS switches and 2) three-dimensional (3-D) MEMS switches. These two architectures are very different in their principle of optical switching, complexities in their mirror control, peripheral electronics, and tolerance requirements in their device fabrication [1].

In the 2-D architecture, mirrors are arranged in a crossbar configuration to perform fully nonblocking switching as shown in Fig. 1. The 2-D optical switches consist of N input and N output ports directed at $N \times N$ array of mirrors. The mirrors have only two states. They can be in the "OFF" position to let light beams pass uninterrupted or in the "ON" position where mirrors move into defined places to reflect light beam in a predetermined direction. As illustrated in Fig. 1, mirror $(m, n,)$ moves into place to reflect light beam from the mth input to the nth output fibers. The digital nature of the mirrors greatly simplifies the control and actuating mechanisms. However, the inherent variations in free space path lengths among port-to-port switching causes variations in optical losses.

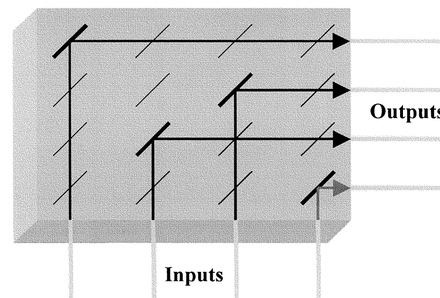

Fig. 1. Conventional crossbar 2-D MEMS switch.

In order to accommodate the relentless needs for higher port-counts, 3-D MEMS switch designs have been proposed [2]. In this architecture, the mirrors can rotate to multiple discrete positions rather than the binary nature of a 2-D MEMS switch. Complicated close-loop servo system with feedback must be implemented for each mirror to move and maintain mirror at desired positions. Therefore, when compared to the 2-D MEMS switches, 3-D MEMS designs are difficult to implement, service, maintain, calibrate, and the associated technical and economical costs are forbiddingly high. The goal of the authors is to address the path dependent optical loss in port-to-port switching of 2-D MEMS switches.

II. L-SWITCHING MATRIX ARCHITECTURE

Like the name suggests, L-switching matrix is shaped like the alphabet "L." The switch architecture is characterized into three quadrants. The most essential portion of the L-switching matrix is the junction quadrant, which consists of double-sided mirrors. As shown in Fig. 2, the junction quadrant is located at the intersection of quadrant I and II. Given N input and N output ports, L-switching matrix utilizes $N^2/4$ double-sided mirrors in the junction quadrant, and $N^2/4$ mirrors in each of the other two quadrants for a total of $3N^2/4$ mirrors. The input ports of the switch are located on the exposed perimeter of the junction quadrant. The mirrors in the junction quadrant direct the light beams into their respective destination quadrants (I or II). Mirrors in quadrant I and II, in turn, redirect the light beams into their respective destination ports.

Manuscript received September 24, 2002; revised January 31, 2003.
The authors are with the Department of Mechanical and Industrial Engineering, University of Toronto, Toronto, ON M5S 3G8, Canada (e-mail: john.yeow@utoronto.ca; eddie.law@utoronto.ca; golden@mie.utoronto.ca).
Digital Object Identifier 10.1109/JSTQE.2003.813310

1077-260X/03$17.00 © 2003 IEEE

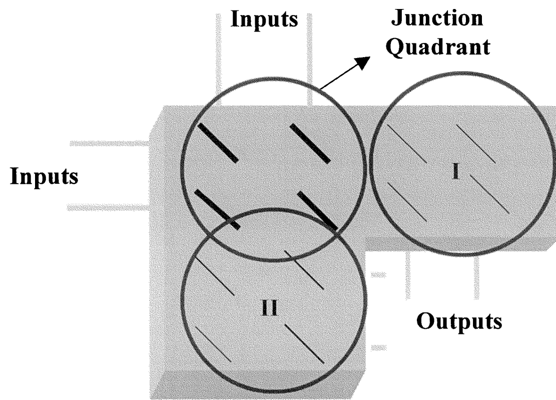

Fig. 2. Architecture of L-switching matrix.

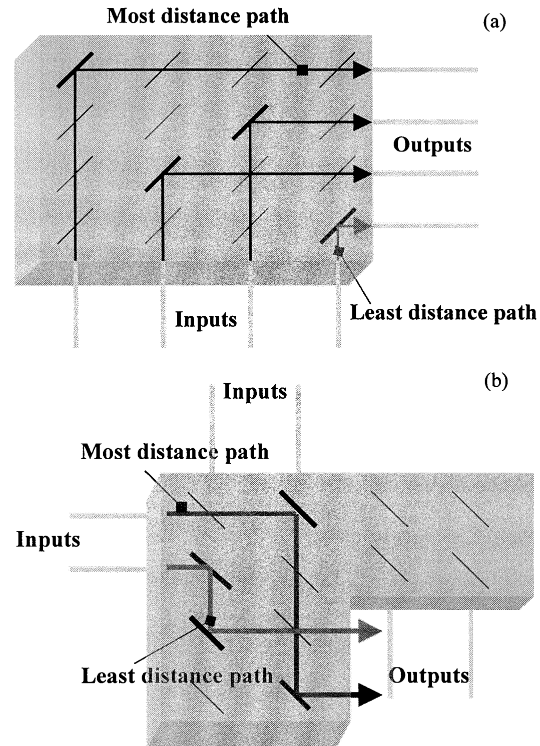

Fig. 3. Path dependency in port-to-port switching in (a) conventional crossbar matrix (b) L-switching matrix.

III. Architectural Comparisons

As reported in many papers on 2-D MEMS switches, performance issues related to the optimum size of mirrors, spacing between mirrors, loss due to angular mirror or collimator misalignment, optimum beam waist size have been systematically addressed [3]. However, one of the most important loss contributors, path length dependent loss, has not been addressed. All of the current 2-D MEMS switches are based on the conventional crossbar architecture as shown in Fig. 1. The problems with the conventional crossbar architecture are twofold: 1) beam waist is selected where the insertion loss is the lowest for the most popular beam path length; therefore, high loss occurs over most and least distance paths and the loss increases as the number of ports increases; and 2) large nonuniform loss between the best and worst coupling paths because of huge differences in its path lengths.

The most and least distance paths of the conventional crossbar architecture are $2N - 1$ and 1 given N as the number of input ports. On the other hand, the most and least distance path of the L-switching matrix are $N + ((N/2) - 1)$ and $((N/2) + 1)$. The L-switching matrix lowers the maximum free-space that light beams travel and hence lowers the loss due to Gaussian divergence. It is also interesting to note that the least distance path is not constant as in the case of the conventional crossbar matrix but is dependent on N. Therefore, the L-switching matrix also decreases the maximum difference in interport optical loss. The maximum path differences of the conventional crossbar and L-switching matrix are $2(N-1)$ and $N-2$. Fig. 3 illustrates the path dependency in port-to-port switching of the conventional crossbar and L-switching matrix. Fig. 5 illustrates the comparison of the maximum distance paths of the conventional crossbar and L-switching matrix. L-switching matrix demonstrates a reduction of the maximum free space propagation path of light by up to 25% over the conventional crossbar architecture. With optimized beam waist size selected such that the insertion loss of the average beam path length is the lowest means that the shorter most and longer least distance paths of the L-switching matrix will minimize the highest loss experienced by the worst coupling path and also improve the loss uniformity experienced by the 2-D MEMS switches. Fig. 6 shows the comparison of maximum path differences of interport switching. Simulation shows that the L-switching matrix has a superior optical performance over the conventional crossbar architecture. The maximum path difference is 50% that of the conventional architecture. Theoretically, twice the current maximum port size, 64×64, is possible with this novel architecture. Pitches shown in the figures are defined as the number of mirror pits a light beam encounters from the input to the output ports. The architecture of L-switching matrix presents an inherent practical problem; the inner output ports of the switch are located in close proximity of each other and their collimators could physically interfere with one another. This problem has to be taken into account during the initial design of the switch. Bulk micromachined Si submount proposed in [13] with micropits and V-grooves could be used to contain micro ball lenses for coupling of light into the output optical fibers. In the 4×4 L-switching matrix prototype, the distance of each pitch is 1500 μm. By using microlenses with diameter of 300 μm as shown in Fig. 4, it should provide sufficient clearance to avoid physical interference between collimators. If larger lenses are used, then a clearance distance (d_c) should be designed into the switch such that any physical interference is avoided. The clearance distance d_c would be a constant added to every path lengths of all input ports, therefore, the effect of the added distance could be minimized if an optimum beam waist size is determined for each input ports. An alternative approach to increasing the port size of optical switches is to interconnect smaller 2-D MEMS switches to form multistage interconnect network such as a Clos network. Simulations have shown that Clos network using the L-switching matrix as submodules have better optical performance over the conventional crossbar switches [4].

Besides the most and least distance paths experienced in port-to-port switching, the frequency with which a certain

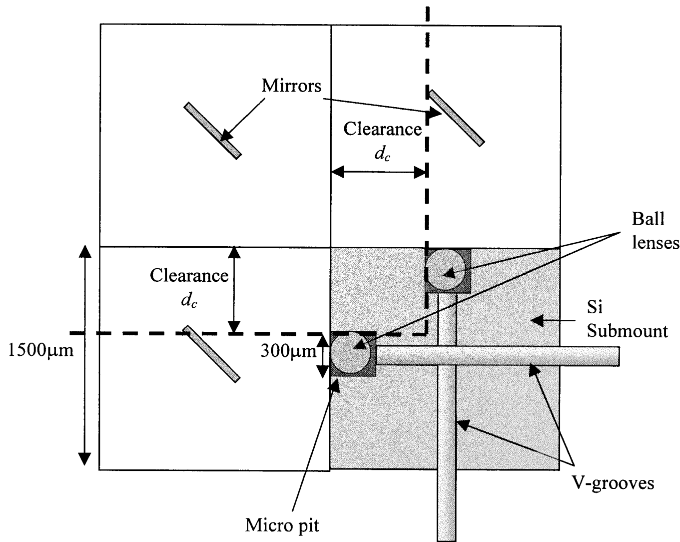

Fig. 4. Si submount with micropits and V-grooves to contain microball lenses and optical fibers.

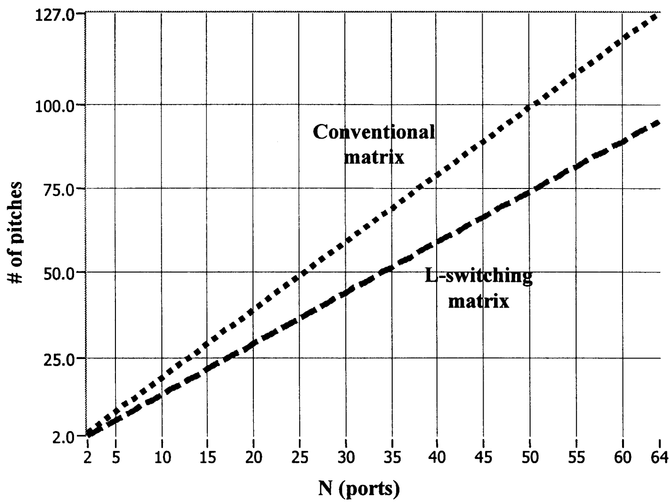

Fig. 5. Most distance paths of conventional crossbar and L-switching matrix.

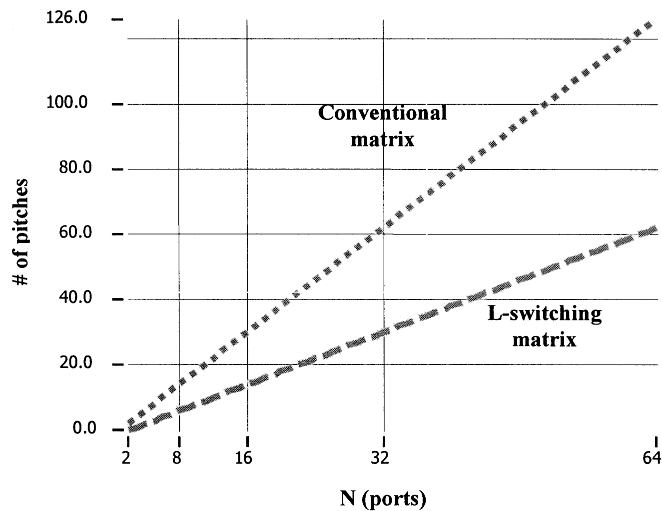

Fig. 6. Maximum path length difference paths of conventional crossbar and L-switching matrix.

length of path is taken is also of interest. It will be beneficial to the overall optical systems performance if this information

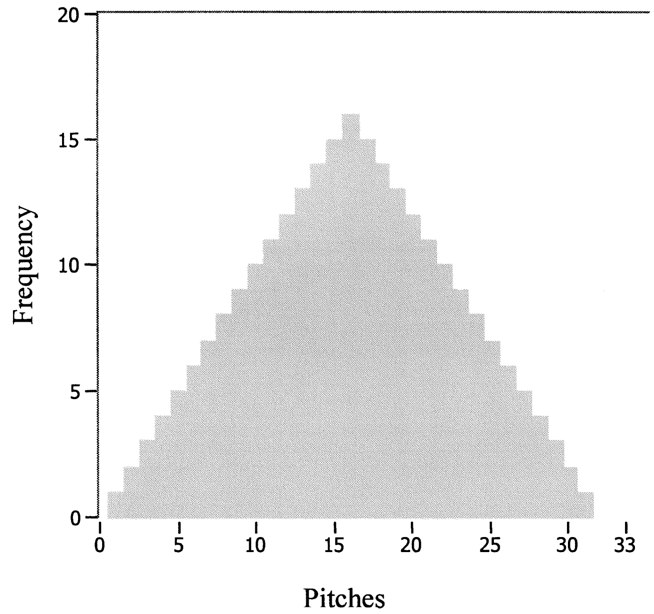

Fig. 7. Histogram of the number of pitches travelled by all 256 paths of a 16×16 conventional crossbar switch.

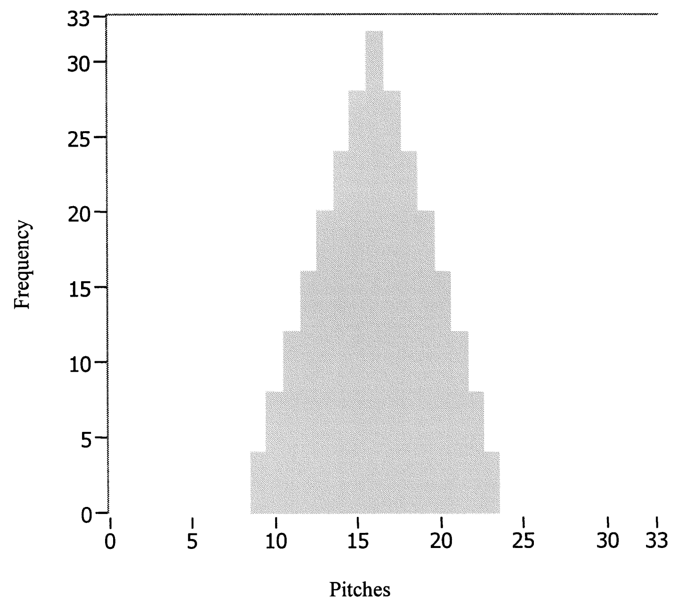

Fig. 8. Histogram of the number of pitches travelled by all 256 paths of a 16×16 L-switching matrix.

is to be taken into account when formulating a solution to compensate for the loss due to Gaussian divergence. Figs. 7 and 8 show the histograms of number of pitches traveled by all 256 paths of a 16×16 conventional crossbar switch and L-switching matrix. The most popular length of light paths is 17 pitches, which occurs 16 times. The least traveled paths are 1 and 31 pitches, both have a frequency of 1. The spread of the path spectrum is wide without one path being dominant. L-switching matrix, on the other hand, has a most popular path length of 16 pitches with 32 occurrences; a minimum path length of nine pitches with four occurrences; and a maximum path length of 23 pitches with four occurrences. The histogram plot of path length frequency of L-switching matrix shows a dominant peak with a narrow spread. In fact, the spread is half

TABLE I
PITCHES TRAVELLED BY INDIVIDUAL INPUTS OF A 16×16 L-SWITCHING MATRIX.

	O^1_{II}	O^2_{II}	O^3_{II}	O^4_{II}	O^5_{II}	O^6_{II}	O^7_{II}	O^8_{II}	O^1_I	O^2_I	O^3_I	O^4_I	O^5_I	O^6_I	O^7_I	O^8_I	Ave
I^1_I	16	17	18	19	20	21	22	23	16	17	18	19	20	21	22	23	19.5
I^2_I	15	16	17	18	19	20	21	22	15	16	17	18	19	20	21	22	18.5
I^3_I	14	15	16	17	18	19	20	21	14	15	16	17	18	19	20	21	17.5
I^4_I	13	14	15	16	17	18	19	20	13	14	15	16	17	18	19	20	16.5
I^5_I	12	13	14	15	16	17	18	19	12	13	14	15	16	17	18	19	15.5
I^6_I	11	12	13	14	15	16	17	18	11	12	13	14	15	16	17	18	14.5
I^7_I	10	11	12	13	14	15	16	17	10	11	12	13	14	15	16	17	13.5
I^8_I	9	10	11	12	13	14	15	16	9	10	11	12	13	14	15	16	12.5

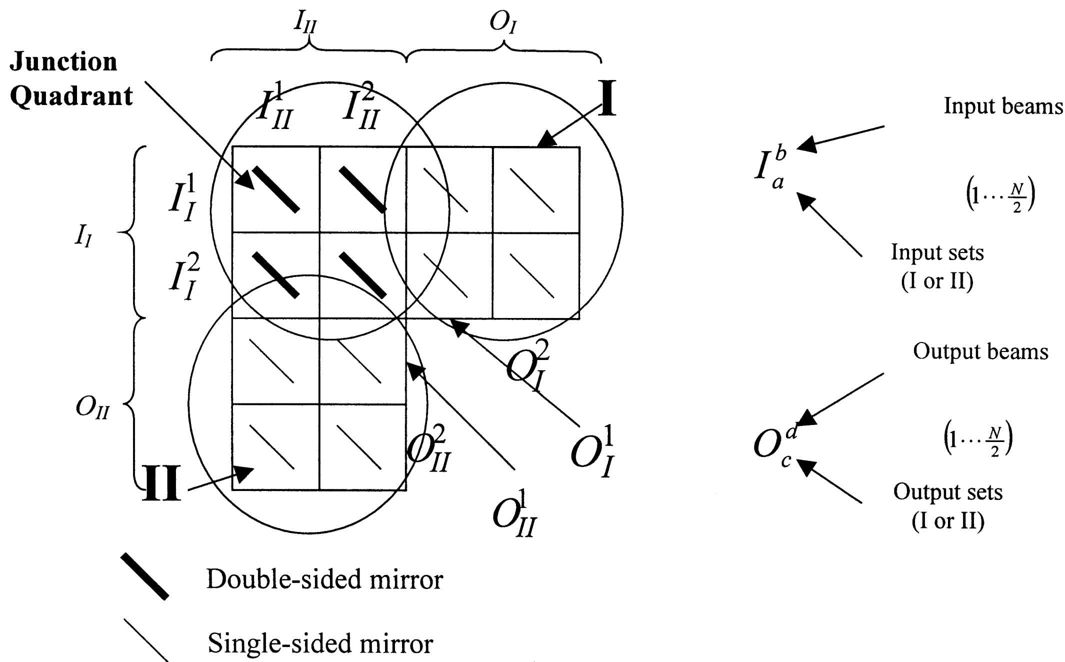

Fig. 9. Input and output sets of L-switching matrix.

that of the conventional crossbar switch. This result is expected given that L-switching matrix is symmetrical diagonally. By designing the minimum beam waist to be located at half the number of most popular pitches, eight in this case, L-switching matrix is expected to have a superior optical performance over conventional crossbar matrix because the variation of the number of pitches within the 256 possible paths is less. Further improvement of the switch can be achieved by analyzing the path length histogram of each input port. The characteristics of the L-switching matrix for the two sets of input are symmetric; therefore, an analysis of one set of input is sufficient. Table I shows the number of pitches traveled by half the inputs to outputs of the L-switching matrix. All possible path lengths of each input port are more confined; therefore, uniformity in loss of individual inputs can be improved greatly by designing beam waists to be located at their average numbers pitches. It should be noted that the occurrence of all path lengths for each input port is two.

IV. MATHEMATICAL MODEL

The input set (I) is divided into two equal sets I_{I} and I_{II}. Similarly, the output set (O) is divided into two equal sets O_{I} and O_{II}. The output set of quadrant I is defined as O_{I}, that of quadrant I_{II} is defined as O_{II}. Each of the input and output sets contains $N/2$ elements. Fig. 9 shows the input and output set definition of L-switching matrix, and the notation of the input and output sets. The coordinate systems of junction I and II quadrants are shown in Fig. 10. Since L-switching matrix is a 2-D MEMS switch, the mirrors have only two states, "ON" or "OFF." Equation (1) states that function which represents light beam "b" of input set I_a has a state of "1" if it is intended for output element "d" of output set O_c , otherwise it has a state of "0." Equation (2) represents the states of the mirrors in the junction quadrant. The states of a mirror are not only dependent on the input or output relationships but also on the states of the mirrors in path traveled by the light beam. Equations (3) and

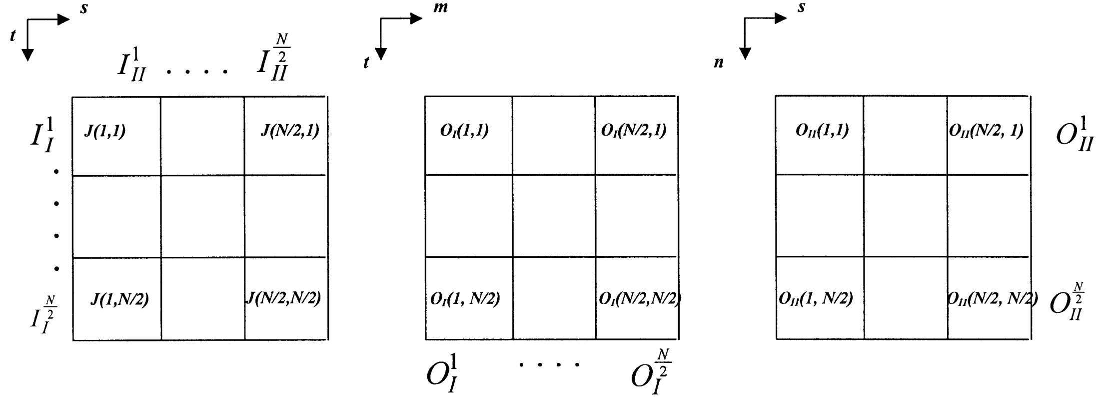

Fig. 10. Coordinate systems of (a) junction quadrant;(b) $O_{\rm I}$ quadrant; and (c) $O_{\rm II}$ quadrant.

(4) describe the states of mirrors in the I and II quadrant. Only the first term of (3) and (4) determine the states of the mirrors when switching from $I_{\rm I}$ set to the I quadrant or $I_{\rm II}$ set to the II quadrant. The second term of the equations describes the states of the mirrors when light is switched from the $I_{\rm II}$ set to the I quadrant or $I_{\rm I}$ set to the II quadrant. In (3) and (4), a state of "1" represents an "ON" state and "0" signifies an "OFF" state. Fig. 11 illustrates the working principle of a 4×4 L-switching matrix.

$$I_a^b\left(O_c^d\right) = 1 \quad \text{if } I_a^b \text{ is intended for } O_c^d \text{ otherwise } 0 \tag{1}$$

$$\begin{aligned} J(s,t) &= \bigcap_{m=1}^{\frac{N}{2}} \overline{I_2^s\left(O_{\rm I}^m\right)} \cap \bigcap_{n=1}^{\frac{N}{2}} \overline{I_1^t\left(O_{\rm II}^n\right)} \\ &\cap \bigcap_{\alpha=1}^{\alpha=s-1} \overline{J(s-\alpha,t)} \cap \bigcap_{\beta=1}^{\beta=t-1} \overline{J\left(s,t-\beta\right)} \end{aligned} \tag{2}$$

$$O_{\rm I}(m,t) = I_1^t\left(O_{\rm I}^m\right) \cup \bigcup_{S=1}^{\frac{N}{2}} J(s,t) I_2^s\left(O_{\rm I}^m\right) \tag{3}$$

$$O_{\rm II}(s,n) = I_2^s\left(O_{\rm II}^n\right) \cup \bigcup_{t=1}^{\frac{N}{2}} J(s,t) I_1^t\left(O_{\rm II}^n\right). \tag{4}$$

V. Device Implementation

The mirrors are supported by a 6-μm-wide torsion bar with a length of 350 μm and thickness of 0.4 μm. A thin torsion bar is fabricated to reduce the required driving voltage. The mirror plates have dimensions of 250 μm by 500 μm with a thickness of 20 μm. The spacing or pitch between mirrors is designed to be 1500 μm. The mirror is rotated about the torsion bars by electrostatic actuation [5]. The electrostatic torque by electrostatic attraction is as expressed as

$$T_e = \frac{\varepsilon}{2} V^2 W \int_0^L \frac{x}{\left\{\left(\frac{d}{\sin\theta} - x\right)\theta\right\}^2}\, dx \tag{5}$$

where

ε $= 8.85 \times 10^{-12}$ F/m is the is the dielectric constant of vacuum;
W width of the mirror;
L length of mirror;
d distance of mirror to grounded bulk Si;
θ angle of rotation;
V applied voltage.

The electrostatic torque is opposed by the mechanical torque of the torsion bars. The mechanical torque serves to restore the mirror back to its original position. The mechanical torque is expressed as [14]

$$T_m = 2 \times \frac{Gwt^3}{3l}\theta\left\{1 - \frac{192}{\pi^5} \cdot \frac{t}{w} \tanh\left(\frac{\pi w}{2t}\right)\right\} \tag{6}$$

where

G is the elastic constant of silicon nitride, 140 Gpa;
l length of torsion bar;
t thickness of torsion bar;
w width of torsion bar;
θ angle of rotation;

$$T_m = T_e. \tag{7}$$

The voltage (V) to rotation angle (θ) has the mirror can be determined using (7). Fig. 12 illustrates the switching actions of a mirror. The mirror is at its initial position "1" when no voltage is applied to the mirror. In this position, light beam is allowed to pass through uninterrupted. Electrostatic fields are created between the mirror and the grounded bulk Si when the mirrors are held at higher voltage potentials. The mechanical torque of the torsion bars opposes the torque generated by the electrostatic fields on the mirror. A voltage higher than the yielding voltage is supplied to the mirror so that the resisting mechanical torque is completely overcame by the electrostatic torque. At this point, the mirror spontaneously rotates to position "2." The stopping angle of the mirrors has to be maintained at 90° for optimum coupling of light into output optical fibers, therefore, alignment of the mirrors to their respective stoppers are critical. SiO_2 is deposited on bulk Si to act as DRIE etch mask for patterning the mirror stoppers and alignment grooves, and also serves as electrical insulation layer. The alignment grooves help the manual alignment of the mirrors to the stoppers under a microscope. Fig. 13 shows the scanning electron microscope

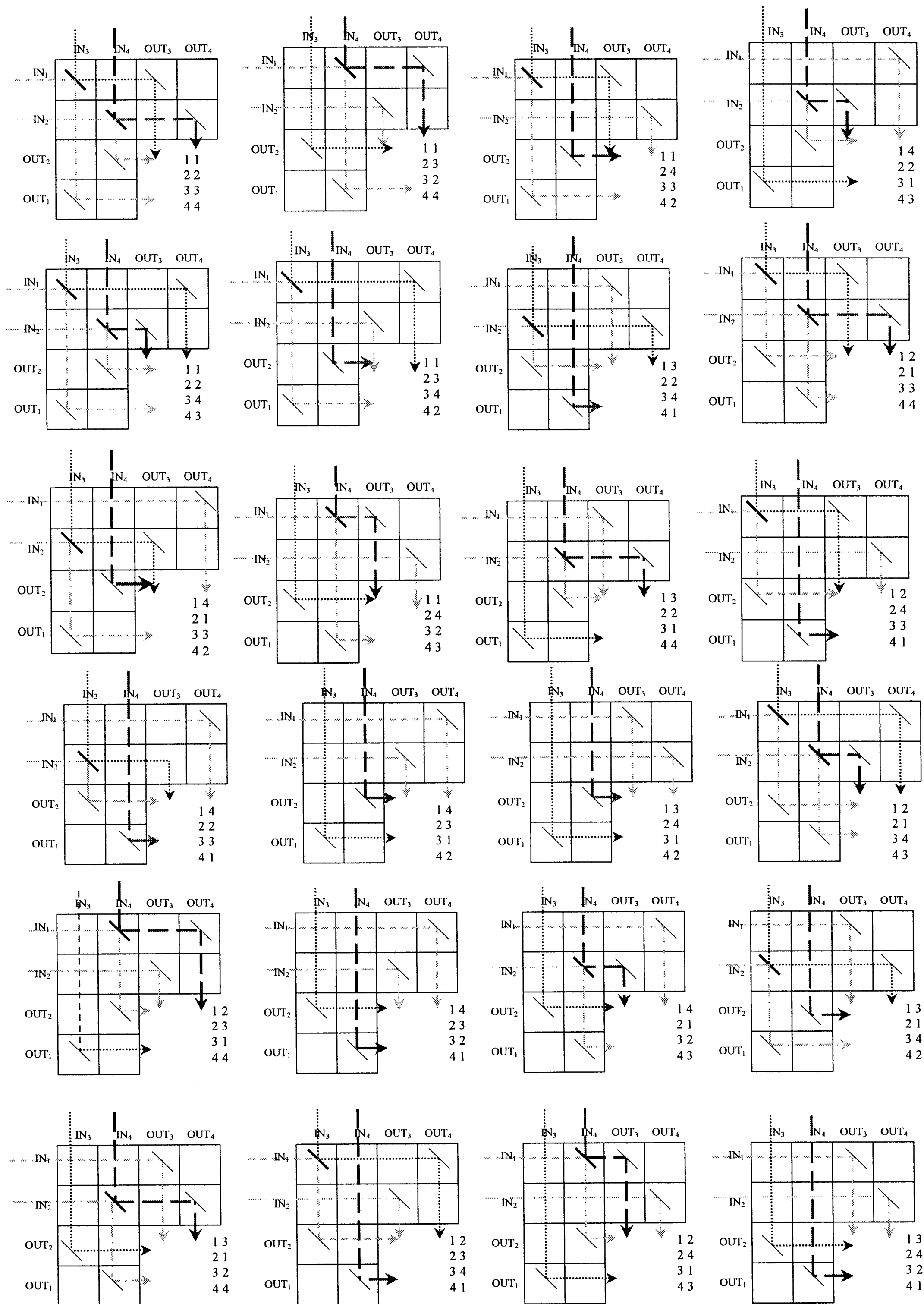

Fig. 11. The 4×4 L-switching matrix operating principle.

(SEM) picture of an array of mirror stoppers, and alignment grooves. Fig. 14 shows an SEM close-up of a stopper with a 45° angled etch.

The L-switching matrix can be implemented by many other actuation mechanisms [6], [7], electrostatic actuation has been chosen because of the simplicity in its implementation. The rotating action of the mirror can also be achieved by other published methods such as a combination of hinge joints and pushrods [8], or combdrive lateral movement [9]. Submillisecond switching rates by MEMS switches has been achieved [10].

A 4×4 L-switching matrix was fabricated using an SOI wafer. An SEM picture of a double-sided mirror and the top view of the L-switching matrix are shown in Figs. 15 and 16.

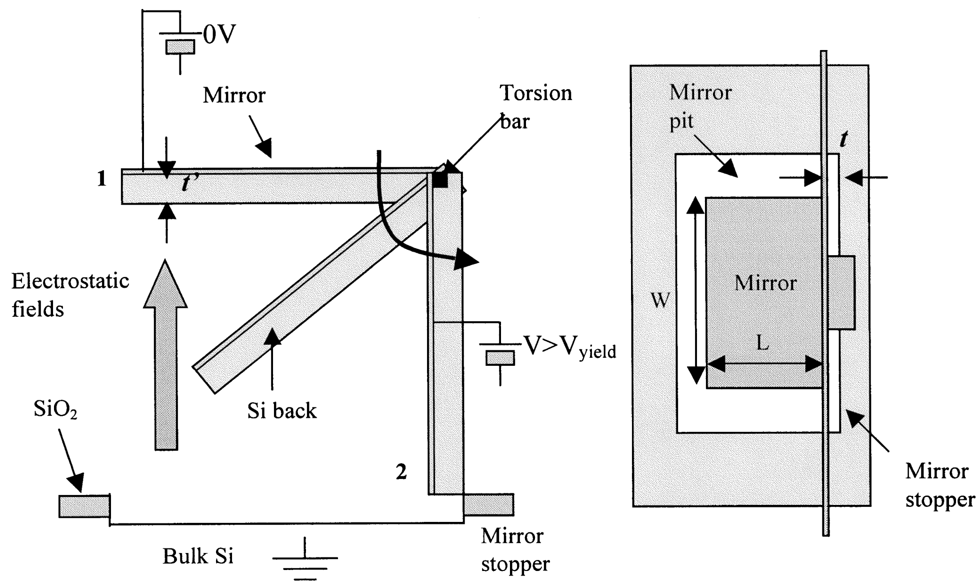

Fig. 12. Operating principle of switching mirror.

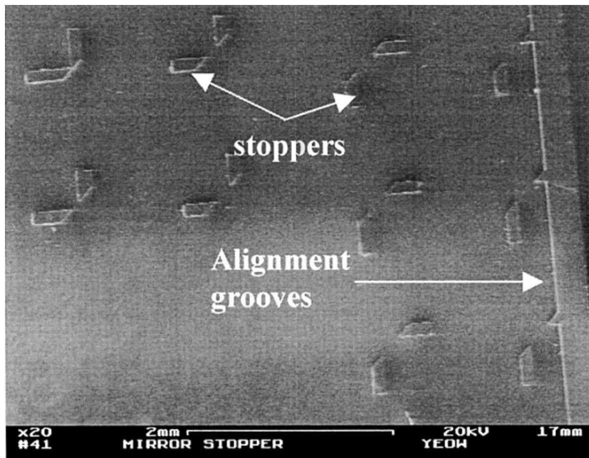

Fig. 13. SEM picture of array of mirror stoppers.

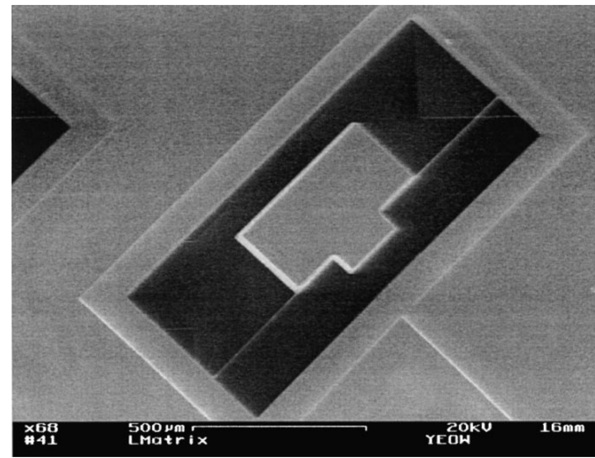

Fig. 15. SEM of a double-sided mirror.

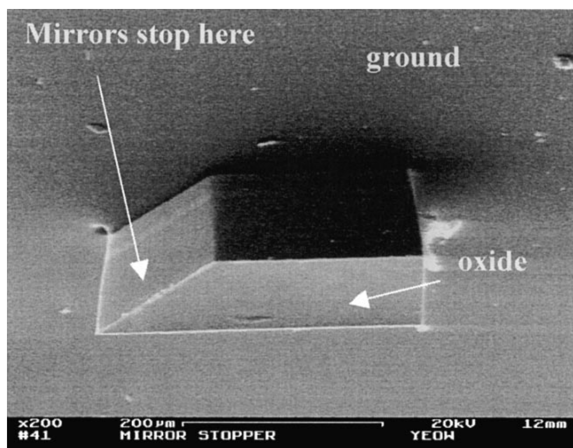

Fig. 14. 45° angled mirror stopper.

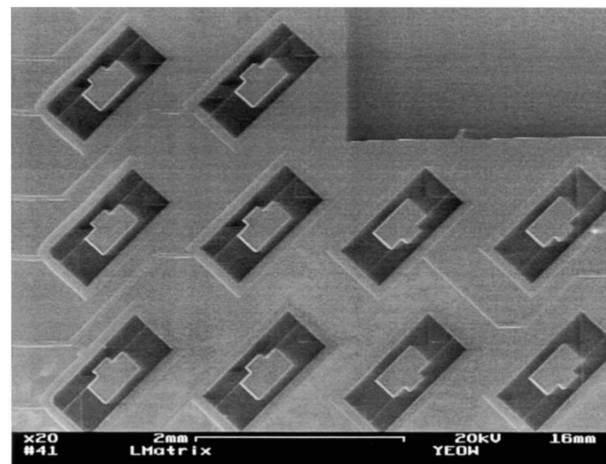

Fig. 16. SEM of a 4×4 L-switching matrix.

The top view and cross section of the fabrication sequence of a double-sided mirror is shown in Fig. 17. The process starts with the following.

a) ⟨100⟩ silicon-on-insulator (SOI) with 20-μm device layer silicon, 0.5-μm buried oxide layer, 300-μm handle Si layer. 0.4 μm of low stress silicon nitride is deposited and

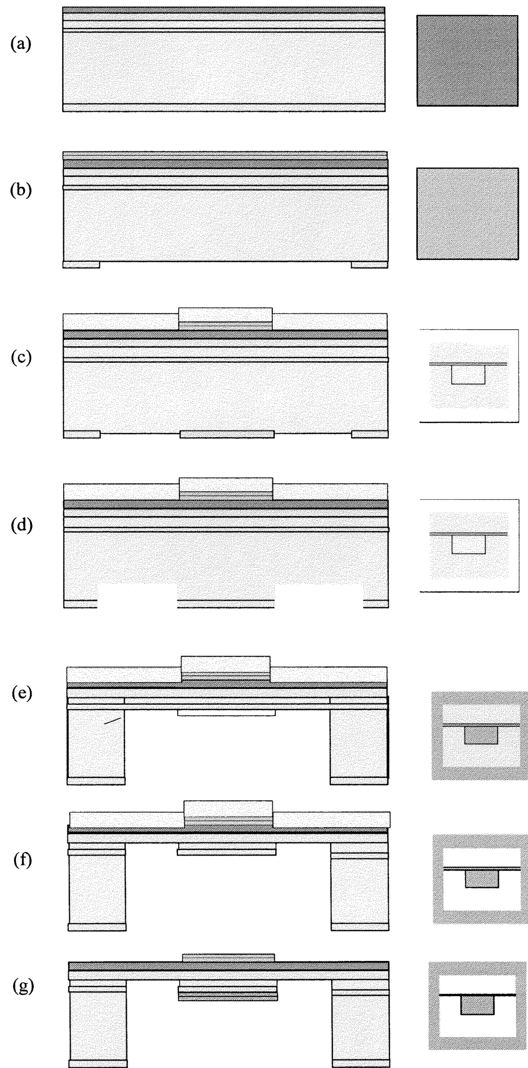

Fig. 17. Fabrication process for L-switching matrix.

patterned by plasma enhanced chemical vapor deposition (PECVD) as torsion bar material and 0.7 μm and 2 μm SiO_2 on the top and backside of SOI. The top layer SiO_2 acts as an insulation layer and the bottom layer acts as etch mask.

b) Cr (0.01 μm) and Al (0.05 μm) metal layers are deposited as the reflective surface of the mirror by vacuum evaporation and the backside of the SOI is patterned and etched by reactive ion etching (RIE) to expose the bulk Si.

c) Al and Cr are stripped to pattern the mirror area and torsion bars. Bottom of wafer is patterned with thick photoresist to act as etch mask during deep reactive ion etching (DRIE) of bulk Si.

d) Etch the bottom side of wafer to form a 20 μm trench around the photoresist. The Si island will act as a protection layer when etching buried oxide and Si device layer in later steps.

e) After stripping the photoresist, continue etching backside of SOI by DRIE until the buried oxide layer is exposed.

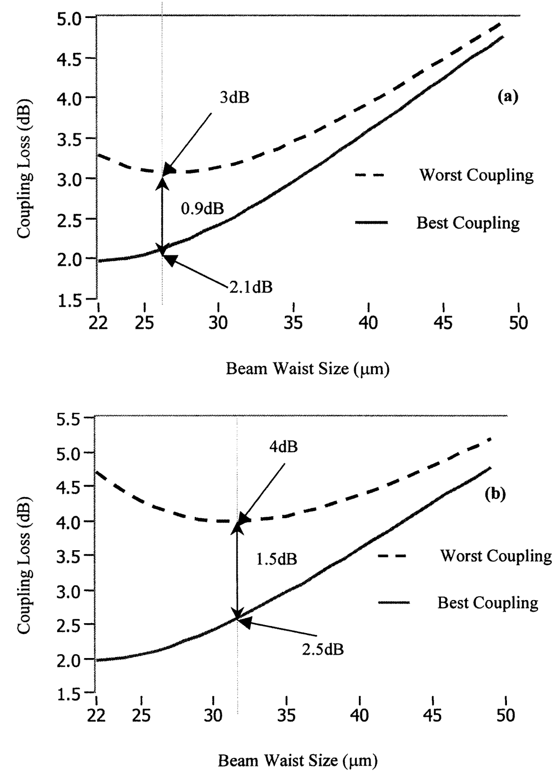

Fig. 18. Theoretical simulation for loss versus beam waist for (a) L-switching matrix, and (b) conventional crossbar switch.

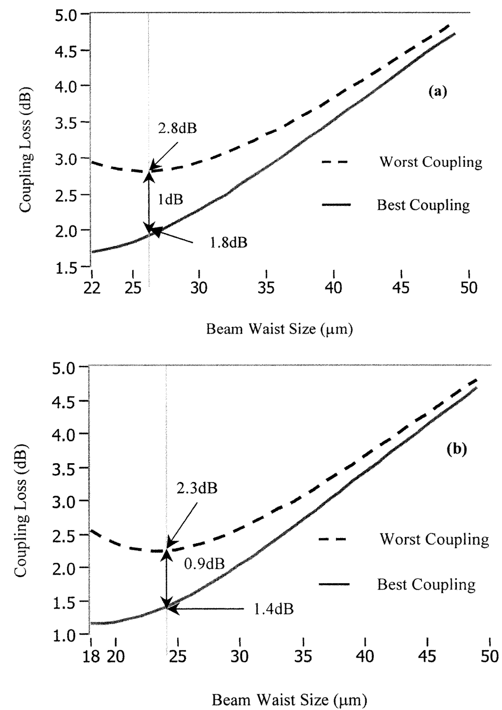

Fig. 19. Theoretical simulation for loss versus beam waist for individual input channels, (a) I_{I}^{1} and (b) I_{I}^{2}.

f) Release the mirror by etching buried oxide layer and the underlying Si device layer by RIE.

g) Deposit Cr (0.01 μm) and Al (0.05 μm) metal layers on the backside of wafer to create a double-sided mirror.

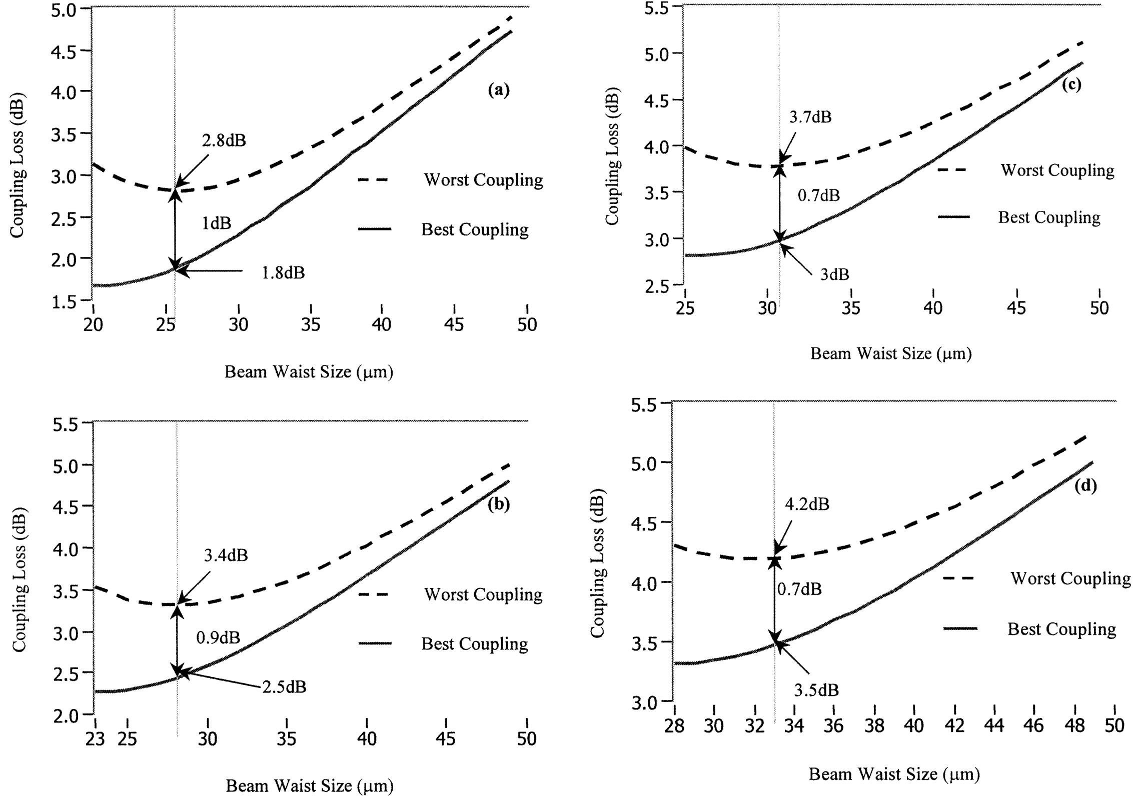

Fig. 20. Theoretical simulation for loss versus beam waist individual input channels of conventional crossbar switch for (a) I_1, (b) I_2, (c) I_3, and (d) I_4.

VI. Experiments and Analysis

A green HeNe laser with a wavelength of 543.5 nm is used as the light source. Laser with wavelength in the visible spectrum is used, instead of conventional telecommunication wavelengths in the range of 1200–1700 nm, to simplify manual fiber alignments. Furthermore, Al maintains good reflectivity into the UV range. The light beam is coupled into a single mode fiber with terminal GRIN len to collimate the output light beam. Experiments show that the loss due mirror reflectivity of topside Al is 1.28 dB. Au could have a reflectivity of 95%, therefore, the use of Au will improve the reflectivity of the mirror. The optical loss of the backside mirror is slightly greater. The measured reflectivity difference between the two surfaces is less than 3%. DRIE has negligible contribution to the front and bottom sides of the mirror surface roughness because they are either protected by photoresist or a patterned Si island during etching. Deposition of metal thin film on two sides of the wafers proves to improve the flatness of the mirror by evening the metal stress distribution on the overall mirror structure. In order to minimize material fatigue of the metal layers during long-term operation of the switch, thickness of Al has been decreased from initial 0.2 to 0.05 μm without severely affecting its reflectivity. At the same time, the reduced thickness also has the effect of reducing polarization dependent loss (PDL).

By employing fiber collimator, losses ranging from 4.5 to 5.2 dB for the longest and short paths have been measured. In the experiments, material reflectivity, beam waist size and position were not optimized to achieve the least insertion loss of the L-switching matrix. The purpose is to demonstrate the working principle and fabrication process of this novel architecture. Optical simulations have been performed to compare the performance of the L-switching matrix with that of the conventional crossbar switch. Fig. 18 shows the theoretical simulation of loss versus beam waist size (by taking into account the) entire path length distribution of a 4×4 L-switching matrix and conventional crossbar switch. When beam waist size is optimized, L-switching matrix has superior optical performance over conventional crossbar switch. (The size and location of the beam waist of) each input port can be individually customized such that its insertion loss is minimized. The characteristics of the two input port sets (I_{I} and I_{II}) of the L-switching matrix are identical; therefore, analysis of any one input set is sufficient. Fig. 19 and Fig. 20 show the loss versus beam waist size for each input port of the two 4×4 switching architectures.

The coupling efficiency Γ is obtained by computing the overlap integral of the amplitude distribution of the divergent Gaussian beam wave function and the nodal wave function describing the receiving optics [11]. Assuming the optics are properly aligned, Γ is expressed as

$$\Gamma = \frac{|\int U^*(x,y,z=d) \cdot U(x,y,z=0)|^2}{|U(x,y,z=d)|^2 \cdot |U(x,y,z=0)|^2} \tag{8}$$

where the integral taken over the aperture of the receiving optics and $U(x,y,z)$ is the lowest-order mode $(\mathrm{TEM}_{0,0})$ of a Gaussian beam [12]. Fig. 21 shows the loss versus path length traversed by all input ports of a 4×4 L-switching matrix. The number of pitches traversed by a 4×4 L-switching matrix ranges from 3 to 5, instead of 1 to 7 for a conventional crossbar matrix. It should be noted that the plotted experimental values

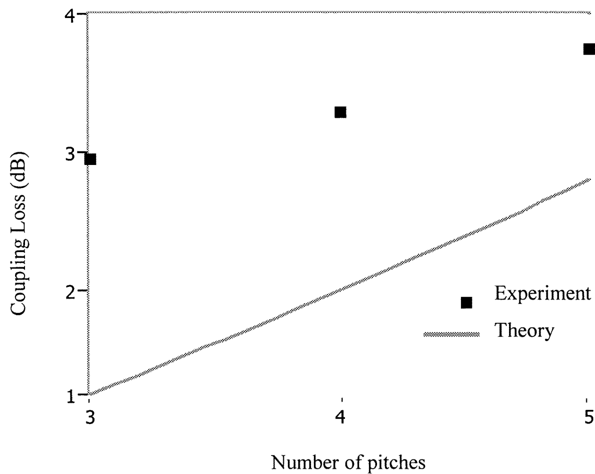

Fig. 21. Theoretical and experimental results on loss versus path length of a 4×4 L-switching matrix.

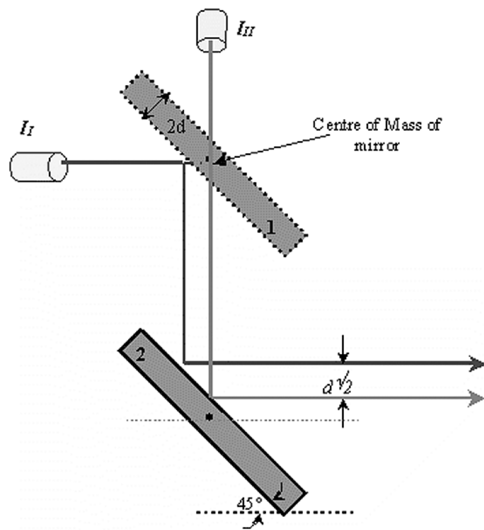

Fig. 22. Spatial shift of light beam due to finite thickness of double-sided mirror.

do not include the 1.28-dB loss due to imperfect reflectivity. The discrepancies between theoretical and experimental results can be attributed to optical misalignment of the receiver optics since the theoretical results assume perfect optical alignment.

Although the L-switching matrix can decrease the absolute and relative paths among port-to-port switching. The penalty for this architecture is the increase in axial misalignment. When the fiber collimators from input insets, $I_{\rm I}$ and $I_{\rm II}$, are aligned with the center of mass of the mirror, the reflected light $(I_{\rm I})$ off mirror 1 will experience a shift in space from the pass-thru light beam of $I_{\rm II}$ due to the finite thickness of the double-sided mirror. The spatial shift is illustrated in Fig. 22. The spatial shift is, however, constant $(d\sqrt{}2)$ and is dependent on the thickness $(2d)$ of the mirror. To minimize the axial alignment, the thickness of the mirror has to be decreased without severely affecting the flatness of the mirror. The contribution of axial misalignment can be determined by performing shifting of the amplitude distribution of the divergent Gaussian beam wave function, $U(x', y, z)$, in the transverse direction. With $d = 10$ μm, the contribution of axial misalignment calculated to be 0.7 dB. 0.2 dB of axial misalignment loss is achievable when $d = 5$ μm.

VII. Conclusion

The path dependent loss of the current 2-D MEMS switches has been addressed. A novel 2-D MEMS optical switch architecture, L-switching matrix, has been proposed, fabricated, and demonstrated. A mathematical model that fully characterizes the new nonblocking architecture for arbitrary $N \times N$ switch has been derived. In order to realize the double-sided mirror of the L-switching matrix, a fabrication process based on SOI wafers has been presented. It is believed that L-switching matrix gives superior optical performance over the conventional crossbar architecture in use today.

Acknowledgment

The fabrication was carried out at the Cornell Nanofabrication Facility (CNF). The authors would like to thank the staffs of CNF for technical supports, and Y. T. Chen of the University of Toronto, and Dr. A. Grave of Nortel Networks for useful discussions.

References

[1] T. W. Yeow, K. L. E. Law, and A. A. Goldenberg, "MEMS optical switches," *IEEE Commun. Mag.*, vol. 39, no. 11, pp. 158–163, Nov. 2001.
[2] A. V. Aksyuk, F. Pardo, C. A. Bolle, S. Arney, C. R. Giles, and D. J. Bishop, "Lucent microstar micromirror array technology for large optical crossconnects," in *Proc. SPIE*, vol. 4178, 2000, pp. 320–324.
[3] L. Y. Lin, E. L. Goldstein, and R. W. Tkach, "Free-space micromachined optical switches for optical networking," *IEEE J. Select. Topics Quantum Electron.*, vol. 5, pp. 4–9, Jan./Feb. 1999.
[4] T. W. Yeow, K. L. E. Law, and A. A. Goldenberg, "Micromachined L-switching matrix," in *Proc. IEEE ICC2002*, vol. 5, 2002, pp. 2848–2854.
[5] H. Toshiyoshi and H. Fujita, "Electrostatic micro torsion mirrors for an optical switch matrix," *J. Microelectromech. Syst.*, vol. 5, no. 4, pp. 231–237, Dec. 1996.
[6] T. Akiyama, D. Collard, and H. Fujita, "Scratch drive actuator with mechanical links for self-assembly of three-dimensional MEMS," *J. Microelectromech. Syst.*, vol. 6, pp. 10–17, 1997.
[7] H. Toshiyoshi, D. Miyauchi, and H. Fujita, "Electromagnetic torsion mirrors for self-aligned fiber-optic crossconnectors by silicon micromachining," *IEEE J. Select. Topics Quantum Electron.*, vol. 5, no. 1, pp. 10–17, Jan./Feb. 1999.
[8] K. S. J. Pister, M. W. Judy, S. R. Burgett, and R. S. Fearing, "Microfabricated hinges," *Sens. Actuators A, Phys.*, vol. 33, pp. 249–256, 1992.
[9] J. A. Yeh, C.-Y. Hui, and N. C. Tien, "Electrostatic model for an asymmetric combdrive," *IEEE/ASME J. Microelectromech. Syst. (JMEMS)*, vol. 9, pp. 126–135, Mar. 2000.
[10] L. Y. Lin, E. L. Goldstein, and R. W. Tkach, "Free-space micromachined optical switches with submillisecond switching time for large-scale optical crossconnect," *IEEE Photon. Technol. Lett.*, vol. 10, pp. 525–527, Apr. 1998.
[11] ——, "On the expandability of free-space micromachined optical crossconnects," *J. Lightwave Technol.*, vol. 18, pp. 482–489, Apr. 2000.
[12] B. E. A. Saleh and M. C. Teich, *Fundamentals of Photonics*. New York: Wiley, 1991.
[13] S. S. Lee, L. S. Huang, C. J. Kim, and M. C. Wu, "Free-space fiber-optic switches based on MEMS vertical torsion mirrors," *J. Lightwave Technol.*, vol. 17, pp. 7–13, Jan. 1999.
[14] S. P. Timoshenko and J. N. Goodier, *Theory of Elasticity*, 3rd ed. New York: McGraw-Hill, 1970.

Tze-Wei Yeow (S'98–M'03) received the B.A.Sc. degree in electrical and computer engineering, the M.A.Sc. in mechanical and industrial engineering, and the Ph.D. degree in robotics and automation from the University of Toronto, Toronto, ON, Canada, in 1997, 1999, and 2003, respectively.

He is currently an Assistant Professor in the department of systems design engineering at the University of Waterloo, Waterloo, ON, Canada. His research interests include developing novel MEMS devices for biomedical imaging and switch architecture for optical cross connects.

K. L. Eddie Law (S'92–M'95) received the B.Sc.(Eng.) degree in electrical and electronic engineering from the University of Hong Kong, the M.S. degree in electrical engineering from the Polytechnic University, Brooklyn, NY, and the Ph.D. degree in electrical and computer engineering from the University of Toronto, Toronto, ON, Canada.

From 1995 to 1999, he was with three different groups—Passport Research Group, Next Generation ATM Systems Department, and Computing Technology Laboratory—in Nortel Networks, Ottawa, ON. Since September 1999, he has been an Assistant Professor in the Communications Group, Edward S. Rogers Sr. Department of Electrical and Computer Engineering, University of Toronto. His current research interests are on active networkings, policy-based management on the Internet, TCP/IP protocol development, and photonic switch design.

Andrew A. Goldenberg (S'73–M'76–M'81–SM'88–F'96) received the B.A.Sc. and M.A.Sc. degrees from the Technion—Israel Institute of Technology, Haifa, in 1969 and 1972, respectively, and the Ph.D. degree from the University of Toronto, Toronto, ON, Canada, in 1976, all in electrical engineering.

From 1975 to 1981, he was with Spar Aerospace Ltd., Toronto, where he worked mainly on control, analysis, design of the space shuttle remote manipulator system, and satellite controls. Since 1987, he has been a Professor of Mechanical Engineering at the University of Toronto. His current research interests include MEMS Sensors-Actuator-Devices with applications in robotics and industrial automation.

Dr. Goldenberg is a former Editor of the IEEE TRANSACTIONS ON ROBOTICS AND AUTOMATION. He is a Member of the American Society of Mechanical Engineers and the Professional Engineers of Ontario.